Table I. ^{95}Mo, ^{14}N, and ^{17}O NMR Data

compd	chem shift, ppm ^{95}Mo[a]	chem shift, ppm ^{14}N[b]	^{95}Mo–^{14}N coupling, Hz	chem shift, ppm $C^{17}O$[c]	chem shift, ppm $N^{17}O$
$(\eta^5\text{-}C_5H_5)Mo(CO)_2(NO)$	−1584 (≤40)[d,j]	38 (50)[e]	46[d]	423 (10)[d]	448 (100)[d]
$(\eta^5\text{-}C_5Me_5)Mo(CO)_2(NO)$	−1404 (≤40)[d,j]	52 (60)[e]	46[f]	424 (10)[d]	454 (120)[d]
$HB(3,5\text{-}Me_2Pz)_3Mo(CO)_2(NO)$	−751 (60)[g,j]	17 (130)[e]	44[h]		
$HB(Pz)_3Mo(CO)_2(NO)$	−672 (70)[g,j]	18 (160)[e]	*i*		

[a] Relative to 2 M Na_2MoO_4 at pH 11; line width in Hz in parentheses. [b] Relative to nitromethane neat. [c] Relative to H_2O. [d] In CH_3CN at 293 K. [e] In CH_2Cl_2/CD_2Cl_2 at 293 K. [f] In CH_3CN at 343 K. [g] In CH_3CN/acetone at 293 K. [h] In DMF at 423 K. [i] Not yet resolved in DMF at 423 K. [j] Line width of the central peak at half-height.

as the rate of electric quadrupole relaxation of the ^{14}N nucleus is increased.[11-14] The line widths as estimated from peak intensities follow the expected 3:2:3 ratio for an intermediate rate of quadrupole relaxation of the ^{14}N nucleus.[15] Similar ^{95}Mo–^{14}N spin–spin coupling was observed in DMF, CH_2Cl_2, and benzene. In higher viscosity solvents, elevated temperatures were required to observe well-resolved triplets. The splittings are field independent,[10] further confirming their origin as spin–spin coupling.

If the $(\eta^5\text{-}C_5H_5)^-$ ligand of **1** is replaced by $(\eta^5\text{-}C_5Me_5)^-$, $HB(3,5\text{-}Me_2Pz)_3^-$, or $HB(Pz)_3^-$, then τ_c increases in the order $(\eta^5\text{-}C_5H_5)^- < (\eta^5\text{-}C_5Me_5)^- < HB(3,5\text{-}Me_2Pz)_3^- < HB(Pz)_3^-$, and elevated temperatures are required to resolve the ^{95}Mo–^{14}N coupling (Table I). The relative order of τ_c for the $HB(3,5\text{-}Me_2Pz)_3^-$ and $HB(Pz)_3^-$ complexes is the opposite of that expected from their molecular weights. The same relative order of τ_c is found from ^{11}B NMR on these two complexes. Different interactions of the complexes with the solvent are one possible explanation for this behavior. For the $HB(Pz)_3^-$ compound the triplet is just beginning to be resolved at 423 K in DMF.

The ^{95}Mo chemical shifts become more deshielded in the order $(\eta^5\text{-}C_5H_5)^- < (\eta^5\text{-}C_5Me_5)^- < HB(3,5\text{-}Me_2Pz)_3^- < HB(Pz)_3^-$. Methylation of the $(\eta^5\text{-}C_5H_5)^-$ ligand causes deshielding whereas methylation of the $HB(Pz)_3^-$ ligand causes more shielding.

The ^{95}Mo–^{14}N spin–spin coupling of 46 Hz was also detected in the ^{14}N NMR spectrum of **1** by using Gaussian multiplication (Figure 1). A sextet of weak satellite peaks is expected in the ^{14}N spectrum from coupling to ^{95}Mo ($I = {}^5/_2$, 15.8% abundant), but the inner two components are obscured by the strong central line for ^{14}N bonded to the molybdenum isotopes with $I = 0$. This central line is broadened by coupling to ^{97}Mo ($I = {}^5/_2$, 9.46% abundant), which has a larger quadrupole moment than ^{95}Mo. The ^{15}N spectrum of **1** in $CDCl_3$ was reported earlier,[16] but no ^{15}N–^{95}Mo coupling was observed.

Replacement of the $(\eta^5\text{-}C_5H_5)^-$ group of **1** by $(\eta^5\text{-}C_5Me_5)^-$ causes a 14 ppm downfield shift of the ^{14}N resonance of the nitrosyl group. The nitrosyl groups of the $HB(3,5\text{-}Me_2Pz)_3^-$ and $HB(Pz)_3^-$ compounds have nearly identical resonances ~20 ppm upfield from **1** (Table I).[17,18]

The ^{17}O chemical shifts for the $(\eta^5\text{-}C_5H_5)^-$ and $(\eta^5\text{-}Me_5C_5)^-$ derivatives are also listed in Table I. No coupling between ^{17}O and ^{14}N was detected. Attempts to observe ^{95}Mo–^{13}C coupling as satellite peaks in the ^{13}C spectra were unsuccessful.

This is the first observation of ^{95}Mo–^{14}N spin–spin coupling. Previously, coupling of ^{95}Mo to ^{17}O,[19] ^{31}P,[2e,h,m,n] ^{19}F,[2n] and ^{13}C[20] has been reported. The observation of ^{95}Mo–^{14}N spin–spin coupling enhances the value of ^{95}Mo NMR as a tool for elucidating the structures of molybdenum compounds and the potential of ^{95}Mo NMR for investigating the binding of nitrogen-containing substrates to molybdenum centers.

Acknowledgment. We thank the U.S. Department of Agriculture for supporting this work under Grant No. 59-2041-1-626 and the National Science Foundation for the purchase of the NMR spectrometer. We thank Dr. C. Brevard at Bruker Spectrospin, SA, Wissembourg, France, for the 400-MHz NMR spectra and his helpful discussions. We also thank Drs. G. Webb and M. Barfield for helpful comments and Dr. R. Richards for a preprint of ref 2u.

Registry No. **1**, 12128-13-1; $(\eta^5\text{-}C_5Me_5)Mo(CO)_2(NO)$, 51213-19-5; $HB(3,5\text{-}Me_2Pz)_3Mo(CO)_2(NO)$, 86272-24-4; $HB(Pz)_3Mo(CO)_2(NO)$, 24981-46-2.

(11) Ogg, R. A.; Ray, J. D. *J. Chem. Phys.* **1957**, *26*, 1515.
(12) Kintzinger, J. P.; Lehn, J. M.; Williams, R. L. *Mol. Phys.* **1969**, *17*, 135.
(13) Shepperd, C. M.; Schaefer, T.; Goodwin, B. W.; T'Raa, J. *Can. J. Chem.* **1971**, *49*, 3158.
(14) Larsen, D. W. *J. Phys. Chem.* **1971**, *75*, 509.
(15) Pople, J. A. *Mol. Phys.* **1958**, *1*, 168.
(16) Botto, R. E.; Kolthammer, B. W. S.; Legzdins, P.; Roberts, J. D. *Inorg. Chem.* **1979**, *18*, 2049.
(17) The $HB(3,5\text{-}Me_2Pz)_3^-$ ligand itself absorbs at −13 ppm with a line width of 850 Hz and is not as easily detected as the nitrosyl group.
(18) For general reviews of nitrogen NMR see: (a) Mason, J. *Chem. Rev.* **1981**, *81*, 205. (b) Witanowski, M., Webb, G. A., Eds. "Nitrogen NMR"; Plenum Press: London, 1973. (c) Witanowsky, M.; Stefaniak, L.; Webb, G. A. *Annu. Rep. NMR Spectrosc.* **1981**, *11B*.
(19) Vold, R. R.; Vold, R. L. *J. Chem. Phys.* **1974**, *61*, 4360.
(20) (a) Braterman, P. S.; Milner, D. W.; Randall, E. W.; Rosenberg, E. *J. Chem. Soc., Dalton Trans.* **1973**, 1027. (b) Gansow, O. A.; Kimura, B. Y.; Dobson, G. R.; Brown, R. A. *J. Am. Chem. Soc.* **1971**, *93*, 5922.

Contribution from the Department of Chemistry, University of Tennessee, Knoxville, Tennessee 37996-1600

Electrochemical Studies of Tetrakis(isocyanide) Rhodium(I) Dimers Containing Bis(diphenylphosphino)methane as the Bridging Ligand

Don R. Womack, Paul D. Enlow, and Clifton Woods*

Received February 23, 1982

Dinuclear rhodium(I) isocyanide complexes have received a great deal of attention since Gray and co-workers[1] reported the hydrogen-generating properties of $[Rh_2(bridge)_4][B(C_6H_5)_4]^2$ (bridge = 1,3-diisocyanopropane). Structurally and electronically similar complexes containing the cation $[Rh_2(RNC)_4(L_2)_2]^{2+}$ (R = alkyl group; L_2 = bis(diphenylphosphino)methane (DPM) or bis(diphenylarsino)methane (DAM) have also been prepared,[2,3] but many of the properties of the DPM and DAM complexes have not been fully explored.

The generation of hydrogen from HCl solutions by the "bridge" complex results in the formation of mixed-oxidation-state oligomeric species.[4] Subsequent photolysis of these oligomers gives $[Rh_2(bridge)_4Cl_2]^{2+}$. This species is also obtained from the oxidative addition of Cl_2 to the parent "bridge"

(1) Lewis, N. S.; Mann, K. R.; Gordon, J. G.; Gray, H. B. *J. Am. Chem. Soc.* **1976**, *98*, 7461.
(2) Balch, A. L. *J. Am. Chem. Soc.* **1976**, *98*, 8049.
(3) Balch, A. L.; Labadie, J. W.; Delker, G. *Inorg. Chem.* **1979**, *18*, 1224.
(4) Sigal, I. S.; Mann, K. R.; Gray, H. B. *J. Am. Chem. Soc.* **1980**, *102*, 7252.

0020-1669/83/1322-2653$01.50/0

complex. The DPM and DAM dimers undergo oxidative-addition reactions with Br_2 and I_2 to give similar rhodium(II) dimers.[2,3] Rhodium(II) dimers containing isocyanide ligands can also be formed from the reaction of rhodium(I) and rhodium(III) monomers, as illustrated in eq 1.[5] The dimer

$$Rh(RNC)_4^+ + Rh(RNC)_4X_2^+ \rightleftharpoons Rh_2(RNC)_8X_2^{2+} \quad (1)$$
$$R = \text{alkyl group, } X = \text{halide}$$

formation involves electron transfer accompanied by transfer of X from one rhodium to another with the simultaneous formation of a Rh–Rh bond.

Even though dinuclear rhodium(I) isocyanide complexes readily undergo electron-transfer reactions, a very limited number of electrochemical studies of dinuclear rhodium(I) isocyanide complexes have been reported.[6,7] with only one report of electrochemical studies of rhodium(I) isocyanide dimers containing DPM or DAM as the bridging ligand. In view of the interest in rhodium(I) isocyanide dimers, we have initiated an electrochemical study of rhodium(I) dimers containing DPM as bridging ligands. We report here some results of these studies for complexes **1–5**.[8]

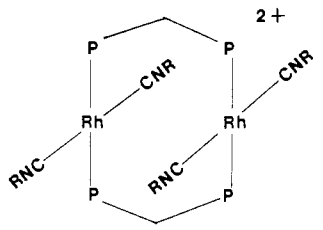

1, R = n-C_4H_9
2, R = i-C_3H_7
3, R = C_6H_{11}
4, R = s-C_4H_9
5, R = t-C_4H_9

Experimental Section

Materials. All tetrakis(isocyanide) rhodium(I) complexes were prepared according to the procedure of Balch.[2] The dichloromethane (Fisher) was spectroanalyzed grade and was used without further purification. The acetonitrile (Aldrich Gold Label) was used without further purification. Tetrabutylammonium hexafluorophosphate (Bu_4NPF_6) was prepared from tetrabutylammonium hydroxide (Bu_4NOH) and HPF_6 in water and was recrystallized three times from acetone–water. Tetrabutylammonium tetrafluoroborate (Bu_4NBF_4) was purchased from Fisher and recrystallized three times from methanol–water and dried under vacuum at 45 °C. All other chemicals and solvents were reagent grade.

Electrochemistry. Cyclic voltammetry was performed with a function generator of the design of Woodward and co-workers[9] and a Princeton Applied Research (PAR) Model 364 polarographic analyzer. The voltammograms were recorded with a Houston Instruments 2000 Omigraphic X-Y recorder. The working electrode was a platinum-inlay electrode (Beckman), and the auxiliary electrode was a platinum grid. The reference electrode was a saturated calomel electrode (SCE). Coulometry and bulk electrolysis experiments were performed with a PAR Model 173 Potentiostat/galvanostat equipped with a PAR 179 digital coulometer. The working electrode for bulk electrolysis was a 25-cm^2 platinum grid, and the axuiliary electrode was a carbon rod. The SCE was the reference electrode. All solutions for electrochemistry were degassed with argon.

Physical Measurements. Ultraviolet–visible absorption spectra were recorded with either a Cary Model 17 or Cary Model 219 spectrophotometer. Infrared (IR) spectra were recorded with a Digilab FTS-20 C/V Fourier transform spectrometer. All analytical determinations were performed by Galbraith Laboratories, Inc., Knoxville, TN.

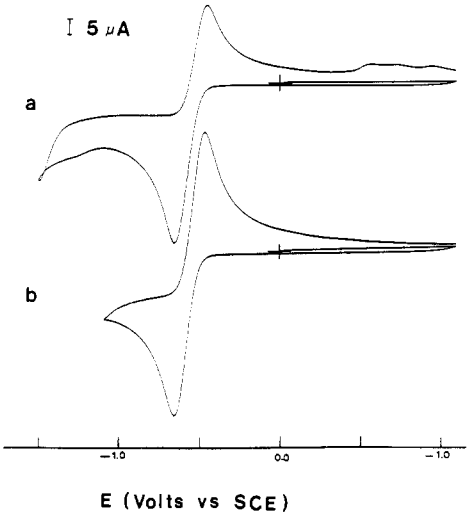

Figure 1. Cyclic voltammograms of $[Rh_2(n\text{-}C_4H_9NC)_4(DPM)_2][PF_6]_2$ in CH_2Cl_2 and 0.1 M Bu_4NPF_6 (sweep rate 100 mV s^{-1}).

Table I. Voltammetric Data for $[Rh_2(RNC)_4(DPM)_2][PF_6]_2$ Complexes[a]

R	E_{pa}	E_{pc}	ΔE	$E_{1/2}$	i_{pc}/i_{pa}
n-C_4H_9	0.67	0.46	0.21	0.57	0.91
i-C_3H_7	0.71	0.52	0.19	0.62	0.93
s-C_4H_9	0.72	0.53	0.19	0.63	0.88
C_6H_{11}	0.71	0.51	0.20	0.61	0.87
t-C_4H_9	0.85	0.62	0.23	0.74	0.92

[a] Sweep rates were 100 mV s^{-1} in CH_2Cl_2 with Bu_4NPF_6 supporting electrolyte. The values for E_{pa}, E_{pc}, ΔE, and $E_{1/2}$ are all reported in volts vs. SCE.

Results and Discussion

One of the principal objectives in exploring the redox chemistry of tetrakis(isocyanide) rhodium(I) dimers was to study the solution behavior of rhodium dimers in new oxidation states. The cyclic voltammetry (CV) technique has been used to characterize the electrochemical behavior of the rhodium dimers.

Electrochemistry in Dichloromethane. The cyclic voltammograms shown in Figure 1 are typical of the tetrakis(isocyanide) dimers in dichloromethane with Bu_4NPF_6 as the supporting electrolyte. Besides that shown in Figure 1a, the only electrochemical activity between +1.50 and −1.50 V is a reduction peak near −1.40 V and its associated oxidation peaks near −0.40 and −0.15 V. Investigations of these processes are in progress and will not be discussed at this time.

When the initial potential scan is in the positive direction out to +1.50 V, two oxidation peaks occur for complexes **1–3**. The second oxidation peak, a small peak near +1.25 V, does not appear for **4** and **5**. The voltammograms of **1–3** show a series of ill-defined reduction peaks between −0.50 and −0.95 V, which are associated with the oxidation peak near +1.25 V. The voltammetric data for the couples illustrated by Figure 1b are presented in Table I. For all complexes in dichloromethane with Bu_4NPF_6 supporting electrolyte, the values of ΔE, the potential separation between the anodic and cathodic peaks, increase as the sweep rate increases. The $E_{1/2}$ values (the mean of E_{pc} and E_{pa}) are essentially independent of sweep rate. This behavior is in accord with a quasi-reversible electron-transfer process.[10,11] A plot of i_{pa} vs. $v^{1/2}$ deviates from linearity over the sweep rate range 20–200 mV s^{-1}. The

(5) Olmstead, M. M.; Balch, A. L. *J. Am. Chem. Soc.* **1976**, *98*, 2354.
(6) Mann, K. R.; Parkinson, B. A. *Inorg. Chem.* **1981**, *20*, 1921.
(7) Fukuzumi, S.; Nishizawa, N.; Tanaka, T. *Bull. Chem. Soc. Jpn.* **1982**, *55*, 2892.
(8) For purposes of clarity, the phenyl groups of the DPM ligands have been omitted.
(9) Woodward, W. S.; Rocklin, R. D.; Murray, R. W. *Chem. Biomed. Environ. Instrum.* **1979**, *9*, 95.
(10) Murray, R. W.; Reilley, C. N. "Electroanalytical Principles"; Interscience: New York, 1963.
(11) Nicholson, R. S. *Anal. Chem.* **1965**, *37*, 1351.

Scheme I

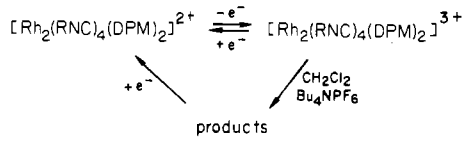

current ratios i_{pc}/i_{pa} are slightly less than 1 for a sweep rate of 100 mV s^{-1}.

When cyclic voltammograms are obtained on solutions of **1–5** at a sweep rate of 100 mV s^{-1} in CH_2Cl_2 and Bu_4NBF_4 supporting electrolyte, the $E_{1/2}$ values are more positive than the $E_{1/2}$ values with Bu_4NPF_6 under the same conditions. The $E_{1/2}$ values for **1–5** with Bu_4NBF_4 are +0.68, +0.71, +0.74, +0.71, and +0.83 V, respectively. The difference of 0.10 ± 0.01 V in $E_{1/2}$ values vs. SCE is due to the different properties of the two supporting electrolytes, as evidenced by a difference of 0.12 V in the ferrocene couple vs. SCE in CH_2Cl_2 for the two supporting electrolytes. The voltammograms of **1–5** in CH_2Cl_2 and Bu_4NBF_4 show one other difference from Figure 1a: the oxidation peak near +1.25 V is more pronounced and well-defined and is now observable for **4**. However, sweeping through these peaks still leads to a series of ill-defined reduction peaks similar to those in Figure 1a. Other than the differences noted, the electrochemical behavior of **1–5** is quite similar in the BF_4^- and PF_6^- systems.

The oxidations associated with the quasi-reversible couples were shown via coulometry to correspond to a one-electron process (n = 1.0 ± 0.1). Controlled-potential electrolysis experiments at potentials 100–200 mV more positive than the peak potentials convert the blue-purple or red-purple solutions to brown-yellow or yellow solutions. Upon complete oxidation, the cathodic peak of the quasi-reversible couple disappears and a series of ill-defined peaks appear at more negative potentials. This behavior indicates that, on the electrolysis time scale, the initial oxidation product undergoes follow-up reactions with the medium to form more stable products. We have not yet been able to identify these products, but it appears that a mixture of products might result. Interestingly, at least some of these products will undergo electrochemical reduction to produce the original purple solutions; thus, the original rhodium(I) species appears to be regenerated. These data support the conclusion that the dimeric framework is not destroyed during the oxidation. Even though the eventual oxidation products have not been identified, the available data are consistent with Scheme I. Since attempts to obtain ESR spectra on the oxidized solution resulted in a very weak and ill-defined resonance, it is possible that the follow-up reactions are types of oligomerization reactions.

The electronic nature of complexes **1–5** is adequately described by the simplified MO diagram in Figure 2.[12] The MO description and the proximity of the rhodium atoms in DPM-bridged dimers suggest that the initial one-electron-oxidation product is probably best described as a Rh(1.5+)–Rh(1.5+) species rather than a Rh(I)–Rh(II) species.

The low-energy electronic transition in the tetrakis(isocyanide) rhodium(I) DPM dimers was previously assigned as a metal-to-ligand charge-transfer transition;[3] however, this transition has been recently reassigned as a $\sigma^*(4d_{z^2}) \rightarrow \sigma(5p_z)$ transition (Figure 2).[12] In the previous study[3] it was observed that a correlation exists between the size of the isocyanide ligand and the wavelength of the lowest energy electronic transition around 520–550 nm. As the steric demands of the isocyanide groups increase, the Rh–Rh separation increases and the interaction between the d_{z^2} orbitals of the two rhodium atoms is reduced as is that between the two p_z orbitals. This

(12) Fordyce, W. A.; Crosby, G. A. *J. Am. Chem. Soc.* **1982**, *104*, 985.

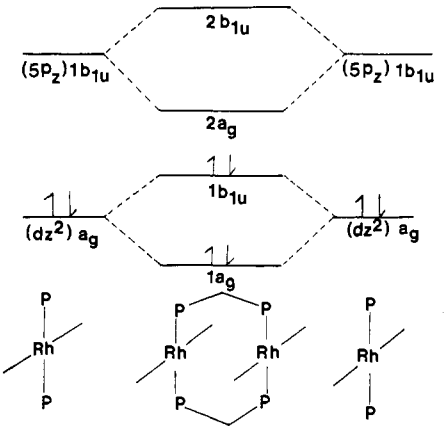

Figure 2. Simplified molecular orbital diagram showing the orbital interactions resulting from face-to-face approach of two square-planar Rh(I) units.

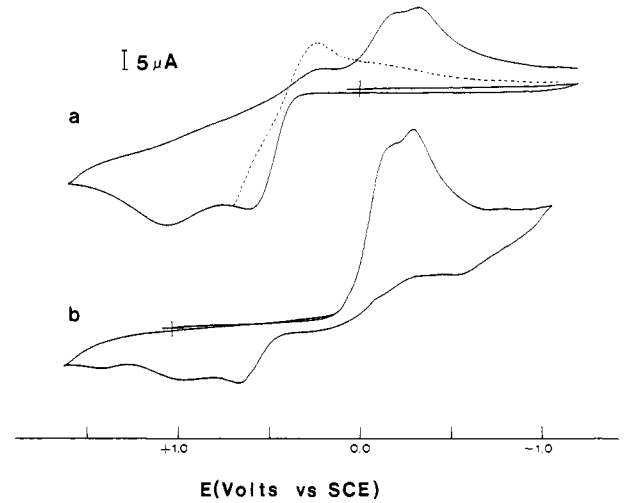

Figure 3. Cyclic voltammograms of $[Rh_2(i\text{-}C_3H_7NC)_4(DPM)_2][PF_6]_2$ (a) before oxidation and (b) after oxidation at +1.00 V in CH_3CN and 0.1 M Bu_4NPF_6 (sweep rate 100 mV s^{-1}).

increases the energy separation of the HOMO and LUMO (Figure 2), moving the transition to higher energy. As the HOMO is stabilized, the oxidation potential should become more positive. The low-energy transitions occur at 546, 545, 548, 538, and 520 nm for **1–5**, respectively, in CH_2Cl_2. A qualitative assessment of the steric requirements of the isocyanide ligands would lead one to conclude that the MLCT transition of **1** should occur at the low end of the MLCT energy range and that of **5** at the high end. Therefore, **1** would be expected to have the least positive $E_{1/2}$ and **5** the most positive. This correlation is observed; however, there does not appear to be an obvious direct relationship between $E_{1/2}$ and λ_{max}, even though a general trend appears to exist. It is possible that electronic factors instead of, or in addition to, steric factors are responsible for the variation in the $E_{1/2}$ values.

Electrochemistry in Acetonitrile. The electrochemistry of complexes **1–5** was investigated in CH_3CN with Bu_4NPF_6 as the supporting electrolyte. A typical voltammogram is shown in Figure 3a and is quite different from the ones obtained in CH_2Cl_2. Two oxidation peaks are observed for all complexes when the initial scan direction is positive. The reduction peaks for **1** and **5** differ slightly from those shown in Figure 3a in the sense that they are not as well-defined. Figure 3a also shows that reversing the sweep before the onset of the second oxidation peak leads to the growth of a peak at +0.24 V (dotted line), which appears to be the cathodic component of a quasi-reversible couple, similar to that observed in the CH_2Cl_2 systems.

Controlled-potential coulometry at +1.30 V corresponds to the total transfer of two electrons (n = 1.94) per dimer cation for the two oxidation processes. If the initial sweep on an oxidized solution of **2** is in the positive direction, the two oxidation peaks no longer appear. When the sweep is reversed at +1.60 V, two reduction peaks occur, one at −0.20 V and one at −0.32 V. On the second positive sweep, two oxidation peaks occur near the potentials of the oxidation peaks of the parent rhodium(I) complex (Figure 3b). An unexplained third oxidation peak also appears. The rhodium(II) dimer formed by oxidizing **1** at +1.00 V in CH_3CN/Bu_4NBF_4 is tentatively assigned structure **6**. The formation of a Rh–Rh bond is

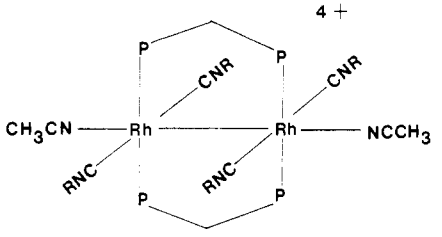

6, R = n-C_4H_9

consistent with other Rh(II)–Rh(II) species[2,3] and makes each rhodium an 18-electron system. When Bu_4NI is added to the oxidized solution containing **6**, the solution turns from yellow to red and the UV–visible spectrum of the resulting solution is identical with that reported[2] for $[Rh_2(n\text{-}C_4H_9NC)_4(DPM)_2I_2][PF_6]_2$, which has been formulated as **7**. This observation supports the conclusion that **6** is the product of the oxidation of **1**.

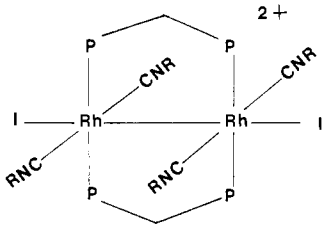

7, R = n-C_4H_9

Acknowledgment. We thank the Research Corp. and Dow Corp. for support of this work. We acknowledge the Instrumentation Division of the NSF for funds that facilitated the purchase of the FT IR spectrometer. P.D.E. thanks the Chemistry Division of Oak Ridge National Laboratory for financial assistance in the form of a graduate stipend. The authors also express their gratitude to Professor J. Q. Chambers (University of Tennessee) for many helpful comments.

Registry No. **1**, 61160-69-8; **2**, 86527-12-0; **3**, 61160-73-4; **4**, 86527-13-1; **5**, 61160-76-7; **6** (X = BF_4^-), 86527-15-3; **7** (X = BF_4^-), 61160-83-6; Rh, 7440-16-6; Bu_4NBF_4, 429-42-5; Bu_4NI, 311-28-4; Bu_4NPF_6, 3109-63-5.

Contribution from the Department of Chemistry, University of New Brunswick, Fredericton, New Brunswick, Canada E3B 6E2

Relationship between the Metal–Metal Distance and the Nature of the Ligands in Dimers Doubly Bridged by Carbonyl, Nitrosyl, or Carbene Groups

Frank Bottomley

Received June 1, 1982

Over the last 15 years a large number of dimeric complexes of general formula $[(L_nM)(L_mM')(\mu\text{-}AB)_2]$ have been prepared, where L is a unidentate or one tooth of a polydentate ligand, n and m are 3 or 4, M and M′ are transition metals (M may be the same as M′), and AB is a bridging ligand in which the atom A actually bridges the metal atoms. The bridging ligand may be a wide variety of π-acceptor or π-donor ligands, but the present analysis is confined to the cases where AB is a π-acceptor ligand, usually CO or NO though methylene bridges are becoming more common. Because we are interested in electronic effects and do not wish to be burdened with steric uncertainties, only dimers in which the two bridging AB ligands are independent will be considered; this precludes acetylene-bridged dimers among others. In Table I are listed the parameters of the 38 dimers of the type under consideration that have been structurally characterized.

Various aspects of these dimers have been discussed previously. In particular, the M–M bond distances and their relation (or lack of relation) to the number of electrons around M has received attention,[1-3] as have the puckering and asymmetry in the $M(\mu\text{-}AB)_2M$ ring.[3] The previous investigations have concentrated on a few of these dimers having closely related structures. We wish here to discuss a more general approach to the M–M and M–A distances in all of the known dimers.

The dimers in Table I fall into three groups. Considering only dimers containing first-row transition metals, inspection of the first four columns of Table I shows that those in group A have M–M distances of 2.36 ± 0.03 Å, M–A distances of 1.82 ± 0.05 Å, and MAM angles of 80.8 ± 2.0°. Dimers in group B have M–M distances of 2.54 ± 0.05 Å, M–A distances of 1.93 ± 0.03 Å, and MAM angles of 82.6 ± 2.0°. Dimers in the third small group, group C, have M–M distances of 2.46 ± 0.06 Å while the M–A distances are markedly unequal on each side of the bridge (unlike dimers of groups A and B) and the MAM angles vary from 68.7 to 86°. The average distances and angles quoted above are simple averages, without taking into account any structural differences between dimers nor correcting for the different covalent radii of M and A. These simple averages are given to show that the dimers fall naturally into three groups without making any assumptions whatever. In order to include the dimers containing Ru in the comparison and to correct for the differences in covalent radii, the M–A distances in group A have been normalized to the Co–C distance in (arbitrarily chosen) $[(Cp^*Co)_2(\mu\text{-}CO)_2]$ by using the covalent radii given in the footnotes to Table I. The normalized distances are given in column 5. For group B $[((OC)_3Co)_2(\mu\text{-}CO)_2]$ was chosen as the standard. Simple normalization of the M–M distance using the metal covalent radii begs the question of whether there is an M–M bond (see below). Since there is no question that an M–A bond exists, the normalized M–M distances (column 6) have been obtained by using the normalized M–A distances and the observed MAM angle. The results of these normalizations are an average M–M distance in group A of 2.38 Å (+0.12, −0.04 Å), an average M–A distance of 1.83 ± 0.05 Å, and an average MAM angle of 81.3° (+2.5, −5.0°). In group B the average M–M distance is 2.55 Å (+0.14, −0.05 Å), the average M–A distance is 1.93 ± 0.03 Å, and the average MAM angle is 82.9° (+4.1, −2.0°).

From the averaged distances and angles the same conclusion is reached as was apparent from the raw data. The M–M and M–A distances in group A are much shorter than in group B. On the other hand, there is no significant difference in the angles, for which the ranges overlap.

(1) Bernal, I.; Korp, J. D.; Reisner, G. M.; Herrmann, W. A. *J. Organomet. Chem.* **1977**, *139*, 321.
(2) Cirjak, L. M.; Ginsburg, R. E.; Dahl, L. F. *Inorg. Chem.* **1982**, *21*, 940.
(3) Pinhas, A. R.; Hoffmann, R. *Inorg. Chem.* **1979**, *18*, 654.

0020-1669/83/1322-2656$01.50/0